2012/06/06
Head Id: 127865
Archive Id: 127843:127887
Archive Date: 2012/06/06
Archive Tag: trunk

Measurement of the top polarization in the dilepton channel

The CMS Collaboration

Abstract

A measurement of top quark polarization in $t\bar{t} \to \ell^+\ell^-$ events is performed in a data sample corresponding to a total integrated luminosity of $5.0\,\text{fb}^{-1}$ collected by the CMS experiment in pp collisions at a centre-of-mass energy of 7 TeV at the LHC. In view of a significant excess reported in the top forward backward asymmetry at the Tevatron, the measured value is compared to the standard model expectation, and is found to be in good agreement.

1 Introduction

Measurements of the $t\bar{t}$ forward-backward asymmentry (A_{fb}) from the Tevatron have led to increased interest in asymmetries in top quark production from both experimentalists and theorists. The results from CDF [1] and D0 [2] show a discrepancy between the measured value of A_{fb} and the predicted value from the standard model (SM). Recent results from CDF [3] report a greater than 3σ discrepancy for events with large $t\bar{t}$ invariant mass. However, a recent paper that uses the the Principle of Maximum Conformality to eliminate the renormalization scale uncertainty gives more accurate values for the SM A_{fb} that differ by only 1σ from the Tevatron results [4].

There are many models of new physics that predict larger values of A_{fb} than in the standard model. This often arises from interference between the standard model and the new physics, where typically top quarks are produced in the exchange of some new heavy particle.

Because the Tevatron is a $p\bar{p}$ collider, there is a natural definition for an asymmetry based on the incoming partons. While the LHC is a symmetric pp collider, it is still possible to measure asymmetries in top quark production. The charge asymmetry, A_C, has been measured at the LHC [5, 6], and no significant deviation from the SM prediction is observed. However, A_C and A_{fb} are in general not tightly correlated, and the top polarization has been identified as an observable where significant evidence of the new physics that could be responsible for the discrepant A_{fb} could be observed [7, 8].

This note presents a measurement of the top polarization in top quark pair production using the full 2011 data set at $\sqrt{s} = 7$ TeV, corresponding to an integrated luminosity of 5.0 fb^{-1}, collected by the Compact Muon Solenoid (CMS) experiment at the LHC. A detailed description of the CMS detector can be found elsewhere [9]. Dilepton decays of the $t\bar{t}$ pair are used, and the top polarization is measured using the reconstructed objects. Because the reconstructed polarization is shaped by the reconstruction efficiency and resolution, we apply an unfolding technique to recover the parton-level distribution which can be compared with theoretical predictions.

2 Event samples, reconstruction, and preselection

The data used for this measurement were collected using one of the ee, eμ, or $\mu\mu$ high-p_{T} double-lepton triggers. Muon candidates are reconstructed using two algorithms that require consistent signals in the tracker and muon systems: one matches the extrapolated trajectories from the silicon tracker to signals in the muon system (tracker-based muons), and the second performs a global fit requiring consistent patterns in the tracker and the muon system (globally fitted muons) [10]. Electron candidates are reconstructed starting from a cluster of energy deposits in the electromagnetic calorimeter. The cluster is then matched to signals in the silicon tracker. A selection using electron identification variables based on shower shape and track-cluster matching is applied to the reconstructed candidates [11]. Electron candidates within $\Delta R \equiv \sqrt{(\Delta\eta)^2 + (\Delta\phi)^2} < 0.1$ from a muon are rejected to remove candidates due to muon bremsstrahlung and final-state radiation. Both electrons and muons are required to be isolated from other activity in the event. This is achieved by imposing a maximum allowed value of 0.15 on the ratio of the scalar sum of track transverse momenta and calorimeter transverse energy deposits within a cone of $\Delta R < 0.3$ around the lepton candidate direction at the origin (the transverse momentum of the candidate is excluded), to the transverse momentum of the candidate.

Event preselection is applied to reject events other than those from $\mathrm{t\bar{t}}$ in the dilepton final state. Events are required to have two opposite-sign, isolated leptons ($\mathrm{e^+e^-}$, $\mathrm{e^\pm\mu^\mp}$, or $\mu^+\mu^-$). Both leptons must have transverse momentum $p_\mathrm{T} > 20\,\mathrm{GeV}/c$, and the electrons (muons) must have $|\eta| < 2.5$ (2.4). The reconstructed lepton trajectories must be consistent with a common interaction vertex. In the rare case ($< 0.1\%$) of events with more than two such leptons, the two leptons with the highest p_T are selected. Events with an $\mathrm{e^+e^-}$ or $\mu^+\mu^-$ pair with invariant mass between 76 and 106 GeV/c^2 or below 12 GeV/c^2 are removed to suppress Drell–Yan (DY) events ($\mathrm{Z}/\gamma^* \to \ell^+\ell^-$) as well as low mass dilepton resonances. The jets and the missing transverse energy $E_\mathrm{T}^\mathrm{miss}$ are reconstructed with a particle-flow technique [12]. The anti-k_T clustering algorithm [13] with a distance parameter of 0.5 is used for jet clustering. At least two jets with $p_\mathrm{T} > 30\,\mathrm{GeV}/c$ and $|\eta| < 2.5$, separated by $\Delta R > 0.4$ from leptons passing the analysis selection, are required in each event. At least one of these jets is required to be consistent with coming from the decay of heavy flavor hadrons and be identified as a b jet by the CSVM b-tagging algorithm [14], which relies on tracks with large impact parameters. The $E_\mathrm{T}^\mathrm{miss}$ in the event is required to exceed 30 GeV, consistent with the presence of two undetected neutrinos.

Signal and background events are generated using the MADGRAPH 4.4.12 [15] and PYTHIA 6.4.22 [16] event generators. For $\mathrm{t\bar{t}}$ events, POWHEG with PYTHIA is used for the $\mathrm{t\bar{t}} \to \ell^+\ell^-$ component, while the remainder, denoted $\mathrm{t\bar{t}} \to$ other is generated using MADGRAPH. The samples of DY with $M_{\ell\ell} > 50\,\mathrm{GeV}/c^2$, diboson (WW, WZ, and ZZ only: the contribution from $\mathrm{W}\gamma$ is assumed to be negligible), and single top quark events are generated using MADGRAPH. The DY event samples with $M_{\ell\ell} < 50\,\mathrm{GeV}/c^2$ are generated using PYTHIA.

Events are then simulated using a GEANT4-based model [17] of the CMS detector, and finally reconstructed and analyzed with the same software used to process collision data. The cross section for $\mathrm{t\bar{t}}$ production is taken from a recent CMS measurement [18], while next-to-leading order (NLO) cross sections are used for the remaining SM background samples.

With the steadily increasing LHC instantaneous luminosity, the mean number of interactions in a single bunch crossing also increased over the course of data taking, reaching about 15 at the end of the 2011 running period. In the following, the yields of simulated events are weighted such that the distribution of reconstructed vertices observed in data is reproduced. The efficiency for events containing two leptons satisfying the analysis selection to pass at least one of the double-lepton triggers is measured to be approximately 100%, 95%, and 90% for the ee, $\mathrm{e}\mu$, and $\mu\mu$ triggers, respectively [19], and corresponding weights are applied to the simulated event yields. In addition, b-tagging scale factors are applied to simulated events for each jet, to account for the difference between b-tagging efficiencies in data and simulation [14].

3 Preselection yields and top polarization at reconstruction level

The observed and simulated yields after the event preselection are listed in Table 1, in which the categories $\mathrm{t\bar{t}} \to \ell^+\ell^-$ and $\mathrm{DY} \to \ell^+\ell^-$ correspond to dileptonic $\mathrm{t\bar{t}}$ and DY decays, including τ leptons only when they also decay leptonically. All other $\mathrm{t\bar{t}}$ decay modes are included in the category $\mathrm{t\bar{t}} \to$ other. The yields are dominated (92%) by top-pair production in the dilepton final state, with the largest background coming from single top production. The $\mathrm{t\bar{t}} \to \ell^+\ell^-$ yields are normalized such that the total simulated yield matches the data. Comparisons between data and the simulation for the number of vertices and the number of b tagged jets are shown in Figure 1.

Table 1: The observed and simulated yields after the preselection described in the text. Uncertainties are statistical only. The systematic uncertainties on the simulated yields are given in Section 7. Where the simulated yields are zero, upper limits are given based on the weighted yield, had one of the simulated events passed the preselection.

Sample	ee	$\mu\mu$	eμ	all
$t\bar{t} \to \ell^+\ell^-$	1791.7 ± 4.4	2127.3 ± 4.7	5069.4 ± 7.3	8988.5 ± 9.7
$t\bar{t} \to$ other	32.5 ± 2.9	4.8 ± 1.1	53.3 ± 3.6	90.7 ± 4.8
W + jets	< 1.9	4.7 ± 3.3	4.7 ± 3.4	9.4 ± 4.7
DY$\to$ ee	52.3 ± 5.8	< 0.6	< 0.6	52.3 ± 5.8
DY$\to \mu\mu$	< 0.6	72.8 ± 6.5	1.6 ± 0.9	74.4 ± 6.5
DY$\to \tau\tau$	17.6 ± 3.3	8.7 ± 2.2	18.7 ± 3.2	45.0 ± 5.1
Di-boson	10.6 ± 0.5	13.0 ± 0.5	24.0 ± 0.7	47.6 ± 1.0
Single top	84.9 ± 2.3	101.2 ± 2.4	252.1 ± 3.9	438.2 ± 5.1
Total (simulation)	1989.6 ± 8.8	2332.6 ± 9.3	5423.8 ± 10.3	9746.0 ± 16.4
Data	1961	2373	5412	9746

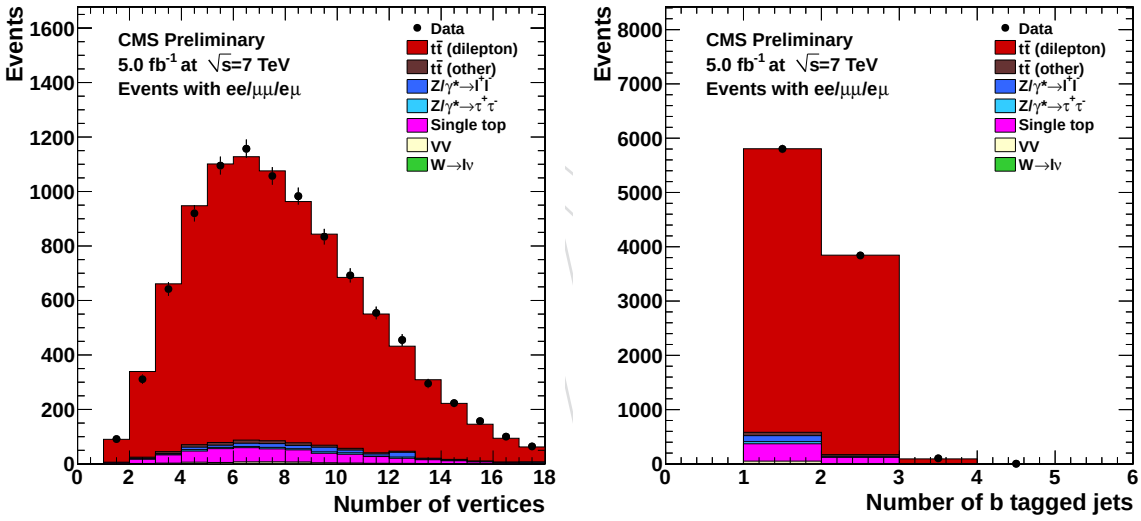

Figure 1: Comparison of data and simulation for number of vertices (left) and number of b tagged jets (right).

The top polarization is defined as

$$P_n = \frac{N(\cos(\theta_l^+) > 0) - N(\cos(\theta_l^+) < 0)}{N(\cos(\theta_l^+) > 0) + N(\cos(\theta_l^+) < 0)},$$

where θ_l^+ is the production angle of the positively charged lepton in the rest frame of its parent top, with respect to the direction of the parent top in the $t\bar{t}$ rest frame.

Measurement of this observable requires reconstruction of the $t\bar{t}$ system. Each event has two neutrinos, and there is also ambiguity in combining b jets with leptons. The analytical matrix weighting technique [20] is used to find a probable solution. Each event is reconstructed using a range of possible M_t values from 100-300 GeV/c^2 in 1 GeV/c^2 steps. The M_t hypothesis with the maximum averaged weight over possible solutions is taken, and the $t\bar{t}$ kinematics are then

taken from the solution with largest weight. Approximately 17% of events have no solution, and are thus not used in the measurement of the top polarization.

A comparison of the $\cos(\theta_l^+)$ distributions in data and simulation is shown in Figure 2. The resulting value of the top polarization P_n at reconstruction level is 0.083 ± 0.011 in data and 0.103 ± 0.002 in the simulation, where the uncertainties are statistical only.

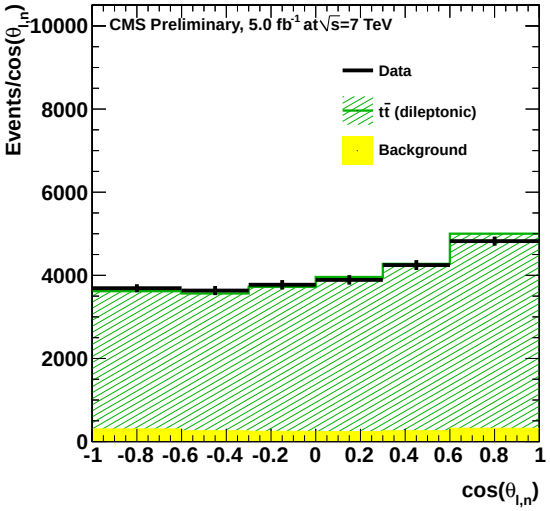

Figure 2: The reconstruction level $\cos(\theta_l^+)$ distribution in the preselection region, for data and the simulation. The simulated events are divided into $t\bar{t} \to \ell^+\ell^-$ and background, where the background consists of the categories other than $t\bar{t} \to \ell^+\ell^-$ in Table 1.

4 Signal regions

After preselection, our sample is dominated by SM $t\bar{t}$ events. To enhance the effect of possible new physics, two signal regions are defined based on the $t\bar{t}$ invariant mass ($M_{t\bar{t}}$) and the sum of the rapidities of the top and anti-top ($|y_t + y_{\bar{t}}|$).

- Signal Region I: $M_{t\bar{t}} > 450$ GeV/c^2.
- Signal Region II: $M_{t\bar{t}} > 450$ GeV/c^2 and $|y_t + y_{\bar{t}}| > 2.0$.

These two regions are interesting because new physics is expected to be more prominent in the high $M_{t\bar{t}}$ region, and the $t\bar{t}$ production from gluon-gluon fusion is significantly suppressed in the forward region.

In the signal regions, the $t\bar{t} \to \ell^+\ell^-$ normalization set in the preselection region is retained. Data yields are compared to the simulation in Tables 2 and 3. The reconstructed polarization in each region is given in Table 4, while a comparison between data and the simulation is shown in Figure 3. Reasonable agreement between the data and the simulated shapes is observed. In Signal Region I there are 5% more events in the simulation than in data, while in Signal Region II the difference is 19%, but the overall normalization has no effect on the measured polarization. The measured polarization is consistent with the simulation in both signal regions.

Table 2: The observed and expected yields in Signal Region *I*. Uncertainties are statistical only. Some of the expected yields are zero due to statistical limitations of the simulated event samples.

Sample	ee	$\mu\mu$	eμ	all
$t\bar{t} \to \ell^+\ell^-$	777.6 ± 2.9	921.4 ± 3.1	2143.0 ± 4.8	3842.0 ± 6.4
$t\bar{t} \to$ other	14.6 ± 2.0	1.5 ± 0.6	23.4 ± 2.4	39.6 ± 3.2
W + jets	0.0 ± 0.0	4.7 ± 3.3	2.8 ± 2.8	7.5 ± 4.4
DY$\to$ ee	13.8 ± 2.9	0.0 ± 0.0	0.0 ± 0.0	13.8 ± 2.9
DY$\to \mu\mu$	0.0 ± 0.0	25.6 ± 3.8	0.5 ± 0.5	26.1 ± 3.9
DY$\to \tau\tau$	7.4 ± 2.2	2.6 ± 1.2	8.0 ± 2.1	18.0 ± 3.3
Di-boson	3.9 ± 0.3	4.7 ± 0.3	9.7 ± 0.5	18.3 ± 0.6
Single top	32.8 ± 1.4	41.9 ± 1.6	101.3 ± 2.5	176.0 ± 3.3
Total (simulation)	850.2 ± 5.3	1002.4 ± 6.3	2288.7 ± 6.9	4141.4 ± 10.7
Data	801	970	2164	3935

Table 3: The observed and expected yields in Signal Region *II*. Uncertainties are statistical only. Some of the expected yields are zero due to statistical limitations of the simulated event samples.

Sample	ee	$\mu\mu$	eμ	all
$t\bar{t} \to \ell^+\ell^-$	104.9 ± 1.1	124.1 ± 1.1	292.2 ± 1.8	521.2 ± 2.3
$t\bar{t} \to$ other	2.8 ± 0.9	0.4 ± 0.3	2.8 ± 0.8	6.0 ± 1.2
W + jets	0.0 ± 0.0	2.2 ± 2.2	0.0 ± 0.0	2.2 ± 2.2
DY$\to$ ee	2.5 ± 1.3	0.0 ± 0.0	0.0 ± 0.0	2.5 ± 1.3
DY$\to \mu\mu$	0.0 ± 0.0	6.5 ± 1.9	0.5 ± 0.5	7.0 ± 2.0
DY$\to \tau\tau$	0.0 ± 0.0	1.0 ± 0.7	0.9 ± 0.7	1.9 ± 1.0
Di-boson	0.7 ± 0.1	0.5 ± 0.1	1.4 ± 0.2	2.5 ± 0.2
Single top	3.7 ± 0.5	5.9 ± 0.6	13.4 ± 0.9	23.0 ± 1.2
Total (simulation)	114.5 ± 1.9	140.7 ± 3.3	311.2 ± 2.3	566.3 ± 4.5
Data	103	116	258	477

Table 4: Reconstructed top polarization in the signal regions. The background is not subtracted, but the contribution of which is small as shown in Figure 3. Uncertainties are statistical only.

Region of P_n measurement	Simulation	Data
Signal Region *I*	0.106 ± 0.003	0.101 ± 0.016
Signal Region *II*	0.069 ± 0.008	-0.006 ± 0.046

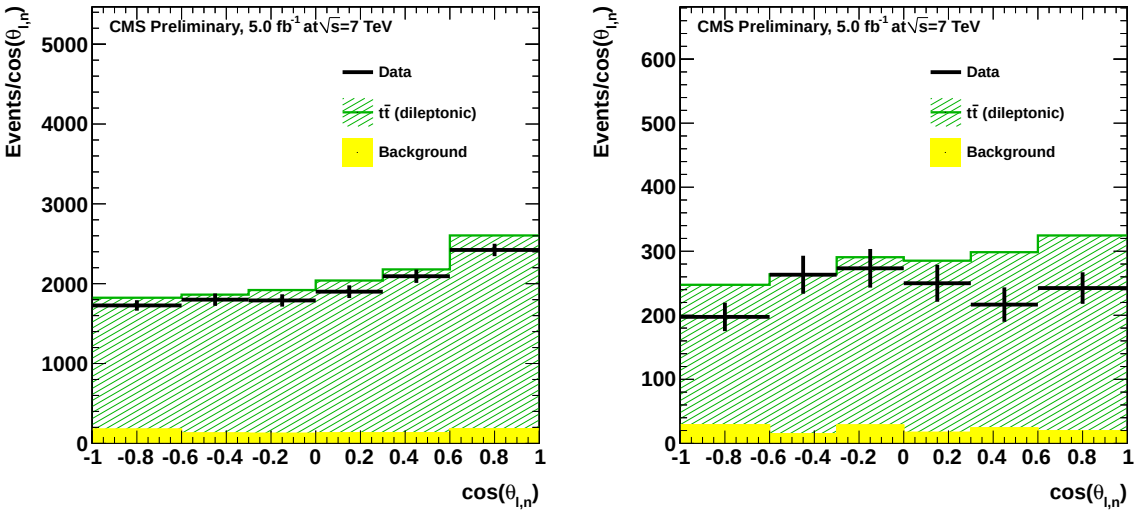

Figure 3: Reconstruction level $\cos(\theta_l^+)$ distributions in Signal Region I (left) and Signal Region II (right). The $t\bar{t} \to \ell^+\ell^-$ normalization is the same as for the preselection.

5 Background estimation

The simulation is used to predict the background event yields and shapes. We use methods based on data to cross-check these estimates for the background contributions from events with misidentified leptons and from DY$\to$ ee/$\mu\mu$ events. However, the dependence of the measured top polarization on the background normalization is small, and in Section 7 the systematic uncertainty is estimated based on changing the normalization of each component by up to 100%.

A misidentified lepton is defined as a lepton candidate not originating from a prompt decay, such as a lepton from semileptonic b or c decays, a muon from a pion or kaon decay, an unidentified photon conversion, or a pion misidentified as an electron. The background from events with misidentified leptons is predicted based on the number of events in data with a candidate lepton that can pass only loosened selection criteria [21]. Using a measurement of the fraction of such "loose" leptons that go on to pass the selection requirements, the number of misidentified leptons in the event sample can be estimated. The resulting prediction is 138^{+281}_{-138} events, including both statistical and systematic uncertainties. The simulated yield is 100.1 ± 6.7, in reasonable agreement.

The estimation method for DY$\to$ ee/$\mu\mu$ events [22] is based on counting the number of Z candidates in the Z veto region (after subtracting the number of non Z events estimated using the number of eμ events), and multiplying this number by the ratio of simulated DY yields outside to inside the Z veto region. The result for the preselection region is an estimate of 142.4 ± 15.0 DY$\to$ ee/$\mu\mu$ events. The result is thus consistent with the simulated prediction of 126.7 ± 8.7 from Table 1.

6 Unfolding

The measured distribution is distorted from the true underlying distribution by the limited acceptance of our detector and the finite resolution of the measurement. The unfolding procedure allows to correct the data for these effects, yielding the "parton-level" $\cos(\theta_l^+)$ distribution and

top polarization. This distribution represents the differential cross-section in $\cos(\theta_l^+)$, and is normalized to unity.

Reconstruction and identification requirements and the kinematic fitter are known to smear out the true kinematics of reconstructed leptons and top quarks. In addition to these smearing effects, the true distribution is also modified by the event selection. If the selection is biased with respect to $\cos(\theta_l^+)$, such bias would cause a change in the observed polarization.

In general, the background-subtracted measured distribution $\vec{b}$ is related to the underlying parton-level distribution $\vec{x}$ by the matrix equation $\vec{b} = SA\vec{x}$, where A is a diagonal matrix describing the acceptance in each bin of the measured distribution, and S is a non-diagonal smearing matrix describing the migration of events between bins due to the detector resolution and reconstruction techniques.

Choice of a binning scheme for the distribution is motivated by the following considerations. Very fine binning would result in large bin-to-bin oscillations caused by statistical fluctuations, while having very few bins is sub-optimal due to reduced information about the smearing. Based on unfolding studies, we find that for our level of statistics, the use of six bins is optimal. The bin size is variable and is chosen to ensure similar level of statistics in each bin of the distribution. A summary of the binning is provided in Table 5.

Table 5: Binning used in the distributions of $\cos(\theta_l^+)$.

B1	B2	B3	B4	B5	B6
[-1.0,-0.6]	[-0.6,-0.3]	[-0.3,-0.0]	[0.0, 0.3]	[0.3, 0.6]	[0.6, 1.0]

The A and S matrices are modeled using the NLO POWHEG-PYTHIA $t\bar{t}$ sample, and are shown in Fig. 4. The smearing effects are quite large due to the uncertainties of top reconstruction. However, most of the large values lie close to the diagonal, meaning there is little extreme smearing between far-apart bins. The distribution is roughly symmetric around the diagonal, indicating that the smearing does not generate artificial asymmetry in reconstructed data, but rather dilutes any existing asymmetry in the true distribution.

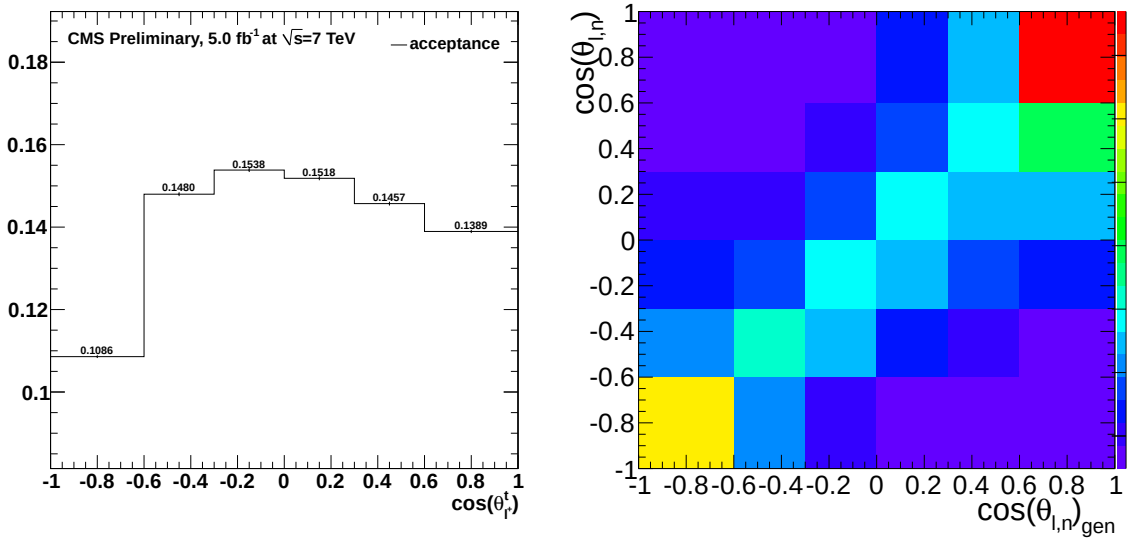

Figure 4: Acceptance matrix bins (left) and smearing effects (right).

We employ a regularized 'unfolding" algorithm based on singular value decomposition (SVD) [23], which is implemented in the RooUnfold package. Effects of large statistical fluctuations in the algorithm are greatly reduced by introducing a regularization term to the unfolding procedure. Regularization strength is defined by the parameter k, which in this measurement is equal to 3. This choice of k was motivated by the effort to maintain balance between the statistical uncertainty of the method and the size of the bias introduced by the unfolding procedure. This is a conservative choice leading to a slightly larger statistical uncertainty compared to choosing a smaller k value, but also reduces the degree to which the corrections tend to bias the result to the response model. The full covariance matrix is used in the evaluation of the statistical uncertainty of the measured asymmetry.

We verify that the unfolding procedure is able to correctly unfold distributions with different levels of asymmetry. In order to do this, we re-weight generated $\bar{t}t$ events according to a linear function of $\cos(\theta_l^+)$: weight=1+$K\cos(\theta_l^+)$. The parameter K is varied between -0.5 and 0.5 in steps of 0.2, introducing a polarization of up to 40%, far more than is expected in $\bar{t}t$ events. For each value of K, we generate 2000 pseudo-experiments, in which the number of events in each bin of the distribution is fluctuated according to Poisson statistics, and then the distribution is unfolded. The average value of the asymmetry in 2000 pseudo-experiments is compared to the original true-level value. We find a linear behavior of this distribution, suggesting that non-SM asymmetry values will also be measured correctly. The offsets and slopes obtained in the linear function fit are -0.004 ± 0.009 and 1.031 ± 0.053, respectively. We also look at the distribution of the pulls in the set of pseudo-experiments and fit it to gaussian function. We find a small bias leading to asymmetry changes of up to 1%, and assign it as an additional systematic uncertainty associated with unfolding bias. The width of the gaussian function obtained in the fit is 0.9, indicating that we slightly over-estimate the measured statistical uncertainty. No correction for this is made.

7 Systematic uncertainties

The systematic uncertainty associated with the jet and $E_{\mathrm{T}}^{\mathrm{miss}}$ energy scale can directly affect the shape of the asymmetry distributions. We evaluate this uncertainty, assuming a 7.5% uncertainty to the hadronic energy scale after jet corrections have been applied [24].

There are also a number of systematic uncertainties due to the background subtraction and unfolding used to produce the parton level measurement. Given the uncertainties of the data driven background estimates described in Section 5, the uncertainty associated with the background estimate is estimated by varying the backgrounds from DY and misidentified leptons by 100%. In addition, we vary the single top background by 50%. The systematic uncertainty from the $\bar{t}t$ modeling is estimated by applying unfolding derived using MC@NLO $\bar{t}t$ to POWHEG-PYTHIA events, and taking the difference in the result compared to that for the POWHEG-PYTHIA derived unfolding. We also assess the systematics due to the shower matching, the top mass, the $b-$tagging, the trigger efficiency, the lepton ID efficiency and the pile-up reweighting. There is a systematic uncertainty of 0.9% to account for the unfolding bias. The systematic uncertainties on the unfolded P_n measurement are summarized in Table 6, combining to a total systematic uncertainty of 0.050.

Table 6: Systematic uncertainties.

	JES	BG	modeling	unfolding	top mass	$b-$tagging	Trigg(lep ID)	PU	Total
P_n	0.043	0.009	0.014	0.009	0.019	0.001	0.000	0.002	0.050

8 Results and summary

The background-subtracted and unfolded $\cos(\theta_l^+)$ distribution for $t\bar{t} \to \ell^+\ell^-$ events is shown in Figure 5. The measured inclusive value of P_n is $-0.035 \pm 0.028 \pm 0.050$ using the preselection events, while the $t\bar{t}$ parton level prediction obtained from POWHEG-PYTHIA simulation is 0.003 ± 0.0004.

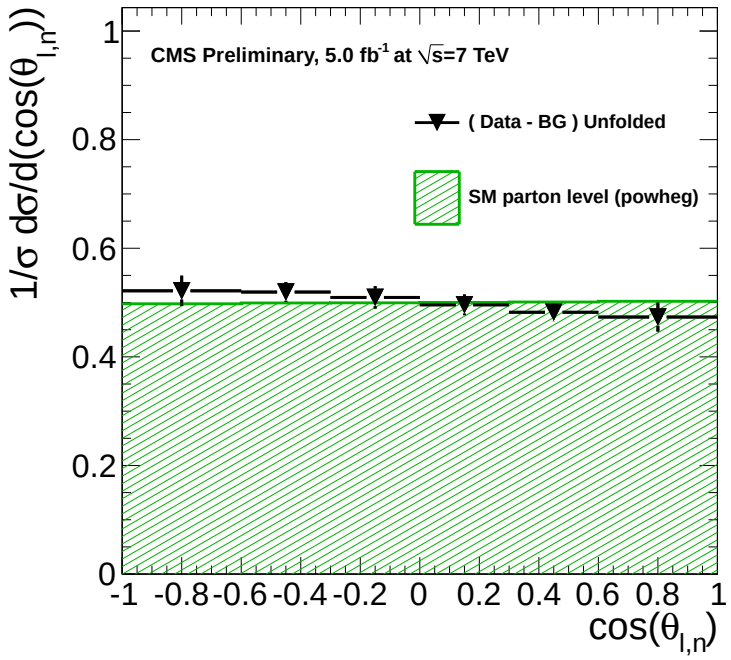

Figure 5: Background-subtracted and unfolded $\cos(\theta_l^+)$ distribution.

The measured value of P_n is consistent with the POWHEG-PYTHIA value, and we thus observe no significant deviation from the SM expectation. We also don't find evidence for new physics in the high $M_{t\bar{t}}$ region ($M_{t\bar{t}} > 450$ GeV/c^2) or the forward region ($|y_t + y_{\bar{t}}| > 2.0$).

References

[1] CDF Collaboration, "Forward-Backward Asymmetry in Top Quark Production in $p\bar{p}$ Collisions at $\sqrt{s} = 1.96$ TeV", *Phys.Rev.Lett.* **101** (2008) 202001, arXiv:0806.2472.

[2] D0 Collaboration, "First measurement of the forward-backward charge asymmetry in top quark pair production", *Phys.Rev.Lett.* **100** (2008) 142002, arXiv:0712.0851.

[3] CDF Collaboration, "Evidence for a Mass Dependent Forward-Backward Asymmetry in Top Quark Pair Production", *Phys.Rev.* **D83** (2011) 112003, arXiv:1101.0034.

[4] S. J. Brodsky and X.-G. Wu, "Application of the Principle of Maximum Conformality to the Top-Quark Forward-Backward Asymmetry at the Tevatron", arXiv:1205.1232.

[5] CMS Collaboration, "Measurement of the charge asymmetry in top-quark pair production in proton-proton collisions at $\sqrt{s} = 7$ TeV", *Physics Letters B* **709** (2012), no. 1-2, 28 – 49, doi:10.1016/j.physletb.2012.01.078.

[6] CMS Collaboration, "Top charge asymmetry measurement in dileptons at $\sqrt{s}$ = 7 TeV", *CMS Physics Analysis Summary* **CMS-PAS-TOP-12-010** (2012).

[7] D. Krohn, T. Liu, J. Shelton et al., "A Polarized View of the Top Asymmetry", *Phys.Rev.* **D84** (2011) 074034, doi:10.1103/PhysRevD.84.074034, arXiv:1105.3743.

[8] J. Drobnak, J. F. Kamenik, and J. Zupan, "Flipping t tbar asymmetries at the Tevatron and the LHC", arXiv:1205.4721.

[9] CMS Collaboration, "The CMS experiment at the CERN LHC", *JINST* **3** (2008) S08004, doi:10.1088/1748-0221/3/08/S08004.

[10] CMS Collaboration, "Performance of muon identification in pp collisions at $\sqrt{s}$ = 7 TeV", CMS Physics Analysis Summary CMS-PAS-MUO-10-002, (2010).

[11] CMS Collaboration, "Electron Reconstruction and Identification at $\sqrt{s} = 7$ TeV", CMS Physics Analysis Summary CMS-PAS-EGM-10-004, (2010).

[12] CMS Collaboration, "Commissioning of the Particle-Flow Reconstruction in Minimum-Bias and Jet Events from pp Collisions at 7 TeV", CMS Physics Analysis Summary CMS-PAS-PFT-10-002, (2010).

[13] M. Cacciari, G. Salam, and G. Soyez, "The anti-k_T jet clustering algorithm", *JHEP* **04** (2008) 063, doi:10.1088/1126-6708/2008/04/063, arXiv:0802.1189.

[14] CMS Collaboration, "Measurement of the b-tagging efficiency using $\mathrm{t\bar{t}}$ events", CMS Physics Analysis Summary CMS-PAS-BTV-11-003, (2011).

[15] J. Alwall, P. Demin, S. de Visscher et al., "MadGraph/MadEvent v4: the new web generation", *JHEP* **09** (2007) 028, doi:10.1088/1126-6708/2007/09/028, arXiv:0706.2334.

[16] T. Sjöstrand, S. Mrenna, and P. Skands, "PYTHIA 6.4 physics and manual", *JHEP* **05** (2006) 026, doi:10.1088/1126-6708/2006/05/026, arXiv:0706.2334.

[17] S. Agostinelli et al., "GEANT4 – a simulation toolkit", *Nucl. Instr. and Meth. A* **506** (2003) 250, doi:10.1016/S0168-9002(03)01368-8.

[18] CMS Collaboration, "Measurement of the $t\bar{t}$ production cross section in pp collisions at 7 TeV in lepton + jets events using b-quark jet identification", *Phys. Rev. D* **84** (2011) 092004, doi:10.1103/PhysRevD.84.092004, arXiv:1108.3773.

[19] CMS Collaboration, "Search for heavy, top-like quark pair production in the dilepton final state in pp collisions at $\sqrt{s} = 7$ TeV", *Submitted to PLB* (2012) arXiv:1203.5410.

[20] CMS Collaboration Collaboration, "Measurement of the t t-bar production cross section and the top quark mass in the dilepton channel in pp collisions at sqrt(s) =7 TeV", *JHEP* **1107** (2011) 049, arXiv:1105.5661.

[21] CMS Collaboration, "Search for new physics with same-sign isolated dilepton events with jets and missing transverse energy at the LHC", *JHEP* **6** (2011) 077, doi:10.1007/JHEP06(2011)077, arXiv:1104.3168.

[22] CMS Collaboration Collaboration, "First Measurement of the Cross Section for Top-Quark Pair Production in Proton-Proton Collisions at sqrt(s)=7 TeV", *Phys.Lett.* **B695** (2011) 424–443, arXiv:1010.5994.

[23] A. Hocker and V. Kartvelishvili, "SVD approach to data unfolding", *Nucl.Instrum.Meth.* **A372** (1996) 469–481, doi:10.1016/0168-9002(95)01478-0, arXiv:hep-ph/9509307.

[24] CMS Collaboration, "Determination of the Jet Energy Scale in CMS with pp Collisions at $\sqrt{s} = 7$ TeV", CMS Physics Analysis Summary CMS-PAS-JME-10-010, (2010).